Modeling impacts of geomagnetic field variations on middle atmospheric ozone responses to solar proton events on long timescales

Holger Winkler,[1] Miriam Sinnhuber,[1] Justus Notholt,[1] May-Britt Kallenrode,[2] Friedhelm Steinhilber,[2,3] Joachim Vogt,[4] Bertalan Zieger,[4,5,6] Karl-Heinz Glassmeier,[7] and Anja Stadelmann[7]

Received 21 February 2007; revised 17 August 2007; accepted 20 September 2007; published 17 January 2008.

[1] Strength and structure of the Earth's magnetic field control the deflection of energetic charged particles of solar and cosmic origin. Therefore variations of the geomagnetic field occurring on geological timescales affect the penetration of charged particles into the atmosphere. During solar proton events (SPEs) the flux of high-energy protons from the Sun is markedly increased. In order to investigate the impact of SPEs on the middle atmospheric ozone on longer timescales, two-dimensional atmospheric chemistry and transport simulations have been performed using simulated time series of SPEs covering 200 years. Monte Carlo calculations were used to obtain ionization rates, which were then applied to the atmosphere under the consideration of different shielding properties of the geomagnetic field. The present-day magnetic field configuration and four other scenarios were analyzed. For the first time, field configurations representing possible realistic situations during reversals have been investigated with respect to SPE-caused ozone losses. With decreasing magnetic field strength the impacts on the ozone are found to significantly increase especially in the Southern Hemisphere, and subsequently, the flux of harmful ultraviolet radiation increases at the Earth's surface. The ozone destructions are most pronounced in the polar regions, and for some field configurations they exceed the values of ozone hole situations after large SPEs. In contrast to ozone holes the depletions due to SPEs are not restricted to winter and spring times but persist into polar summer.

Citation: Winkler, H., M. Sinnhuber, J. Notholt, M.-B. Kallenrode, F. Steinhilber, J. Vogt, B. Zieger, K.-H. Glassmeier, and A. Stadelmann (2008), Modeling impacts of geomagnetic field variations on middle atmospheric ozone responses to solar proton events on long timescales, *J. Geophys. Res.*, *113*, D02302, doi:10.1029/2007JD008574.

1. Introduction

[2] It is well established that solar proton events (SPEs) are sources of distinct chemical disturbances in the middle atmosphere (stratosphere and mesosphere). The pioneering works were those of *Swider and Keneshea* [1973] and *Crutzen et al.* [1975]. Through collisional interactions with air molecules the precipitating energetic protons lose kinetic energy and produce a number of partly ionized atomic and molecular fragments, and energetic secondary electrons cause further dissociations and ionizations. Protons occurring in SPEs typically have kinetic energies between several tens of keV and many hundred MeV. Most important in terms of middle atmospheric impacts are the protons in the energy range from 10 to 500 MeV, of which the most energetic ones can reach the tropopause. For characteristic protons' energy spectra the bulk of ion production takes place in the upper part of the middle atmosphere. Because of the large atmospheric abundance of molecular nitrogen and oxygen, initially, mainly N_2^+, O_2^+, N^+, O^+, and atomic oxygen and nitrogen are produced. Subsequent rapid ion-neutral reactions and recombinations lead to the formation of NO_x (= N, NO, NO_2) [*Crutzen et al.*, 1975; *Porter et al.*, 1976; *Rusch et al.*, 1981]. Additionally, HO_x (= H, OH, HO_2) is being produced by reactions involving ionic water clusters [*Swider and Keneshea*, 1973; *Solomon et al.*, 1981]. Both NO_x and HO_x are well known for their ability to destroy the ozone in catalytic cycles. Furthermore, there is

[1]Institute of Environmental Physics, University of Bremen, Bremen, Germany.
[2]Department of Physics, Universität Osnabrück, Osnabrück, Germany.
[3]Now at Swiss Federal Institute of Aquatic Science and Technology (Eawag), Dubendorf, Switzerland.
[4]School of Engineering and Science, Jacobs University Bremen, Bremen, Germany.
[5]Geodetic and Geophysical Research Institute, Hungarian Academy of Sciences, Sopron, Hungary.
[6]Now at Department of Atmospheric, Oceanic and Space Sciences, University of Michigan, Ann Arbor, Michigan, USA.
[7]Institut für Geophysik und Meteorologie, Technische Universität Braunschweig, Brunswick, Germany.

0148-0227/08/2007JD008574

atomic oxygen released [*Porter et al.*, 1976] which directly affects the odd oxygen chemistry. As a result the ozone chemistry can be significantly disturbed by SPEs. The HO_x-caused O_3 destruction is very effective in the upper part of the middle atmosphere (above about 40 km) [*Nicolet*, 1970; *Lary*, 1997]. Because of their high reactivity the produced HO_x species have a relatively short lifetime, and transport processes are of minor importance for them. In contrast to that, enhanced NO_x concentrations can remain at high levels for several weeks or even months after a SPE, provided that destruction through solar radiation is small. This is especially the case under polar night conditions which at the same time cause pronounced downward transport by descending air masses. These dynamical issues in combination with the longer lifetimes at high solar zenith angles enable NO_x to be transported downward quite effectively [*Jackman et al.*, 1990; *Randall et al.*, 2001] and to cause significant upper stratospheric ozone depletions months after an event [*Jackman et al.*, 2000]. In terms of transport it is useful to consider the odd nitrogen $NO_y = NO_x + NO_3 + HNO_3 + HO_2NO_2 + ClONO_2 + 2 \times N_2O_5$ instead of NO_x as it contains basically all reactive nitrogen species. In various studies the impacts of several large SPEs on the middle atmosphere have been analyzed. The formation of NO_x and the subsequent O_3 destruction have been measured during a number of large SPEs, and the findings are in accordance with results from atmospheric chemistry models [e.g., *Solomon et al.*, 1983; *Jackman et al.*, 2001; *Verronen et al.*, 2005; *Rohen et al.*, 2005].

[3] There are fewer investigations concerning the SPE-caused HO_x perturbations; for example, indirect observations are presented by *von Clarmann et al.* [2005]. In the study of *Verronen et al.* [2006], convincing agreements of model predictions with Microwave Limb Sounder hydroxyl measurements for the SPE in January 2005 are presented, and *Seppälä et al.* [2006] have found that model results in terms of ozone destruction by HO_x in the mesosphere during a SPE are confirmed by global ozone monitoring by occultation of stars (GOMOS) data. Anyway, for the purpose of longer-term effects on ozone, as they are addressed here, the HO_x contribution is of minor importance.

[4] The quoted comparisons with measurements give confidence in the tools for modeling the atmospheric impacts of SPEs focusing on ozone destruction so that it appears justified to use them for the investigations presented here. The atmospheric chemistry model is described in section 2.2.

[5] The regions in which extraterrestrial charged particles actually can enter the atmosphere are determined by their deflection and guidance by the geomagnetic field. Thus they depend on both the particle's energy as well as on the structure of the Earth's magnetic field. Because of its dipole topography the present geomagnetic field allows protons in the SPEs' energy range to enter the Earth's atmosphere only in the (magnetic) polar regions. To a good approximation this can be described by an energy-independent cutoff latitude λ_c (i.e., the geomagnetic latitude which defines the edge of the magnetically open polar cap regions). *Jackman et al.* [2000, 2005] use a cutoff latitude of 60°, noting that actual values can differ from that depending on the spectrum of the solar protons. In general, higher particle energies correspond to smaller cutoff latitudes, and λ_c is depressed by geomagnetic disturbances which are often associated with Earth's directed SPEs. For the large SPE in August 1972 a value of 58° for λ_c was determined by *Reagan et al.* [1981]. Such values correspond to a rather strong coupling between the solar wind and the magnetosphere [*Siscoe and Chen*, 1975] which are indeed not unrealistic during and right after large SPEs. More recently, *Birch et al.* [2005] have investigated variations in λ_c during three SPEs in the year 2001, exploiting proton-counting rates from polar-orbiting satellites. Their finding was that the cutoff latitude varies around 60° and decreases by up to 10° during the observed SPEs. They also report small diurnal variation. Nevertheless, on average, $\lambda_c = 60°$ seems to be a reasonable assumption for the current magnetic field.

[6] The terrestrial magnetic field is not static. As mentioned above, solar wind variations have an influence on its structure on timescales from hours up to years. Of greater interest for our study are the slower variations of the Earth's internal magnetic field which can greatly alter the shape of the magnetosphere and with that its shielding properties against charged extraterrestrial particles. Within the last 400 years the magnitude of the Earth's magnetic dipole term has decreased quite significantly by about 39% [*Fraser-Smith*, 1987]. On longer timescales, even more pronounced changes of both the geomagnetic field strength and its topology occur [see, e.g., *McElhinny and Senanayake*, 1982]. The terrestrial magnetic field has changed its polarity many times at irregular intervals of about 250,000 years throughout geological history. During such a field reversal the dipole component is depressed to lower than 25% of the present value for several thousand years, and then the field is no longer dominated by its dipole component [*Merrill and McFadden*, 1999]. Long-term effects of the changing geomagnetic fields with respect to space climatology were studied by *Glassmeier et al.* [2004]. *Sinnhuber et al.* [2003] have investigated the extreme case effect of a completely vanishing magnetic field on chemical SPE impacts in the middle atmosphere. They found that the atmospheric disturbances caused by large SPEs strongly increase if there is no magnetic shielding applied at all. Then losses of total ozone reach up to 50% in polar regions, and erythemal weighted UVB increases in midlatitudes by about 10%. However, the assumption of an atmosphere entirely exposed to energetic solar protons is an absolute extreme case and quite unlikely. In order to regard more realistic scenarios it is necessary to consider the nature of the Earth's magnetic field specifically. Details about geomagnetic field variations can be derived from the worldwide analysis of paleomagnetic proxy data [e.g., *Mankinen and Dalrymple*, 1979]. The last full polarity reversal, the Matuyama/Brunhes transition, occurred about 780,000 years ago. It is clearly recorded in volcanic and marine material from which the global magnetic field can be reconstructed [e.g., *Guyodo and Valet*, 1999]. A complementary approach to investigate reversals is the analysis of the mechanisms of field generation in the Earth's core. Detailed numerical simulations [e.g., *Glatzmaier and Roberts*, 1995; *Wicht and Olson*, 2004] have led to a better understanding of the so-called geodynamo. Both reconstructions from paleomagnetic proxy data and modeling of the geodynamo indicate that the field's structure during reversals has significant nondipolar contributions. More polarity transitions are expected during periods of weak field intensity

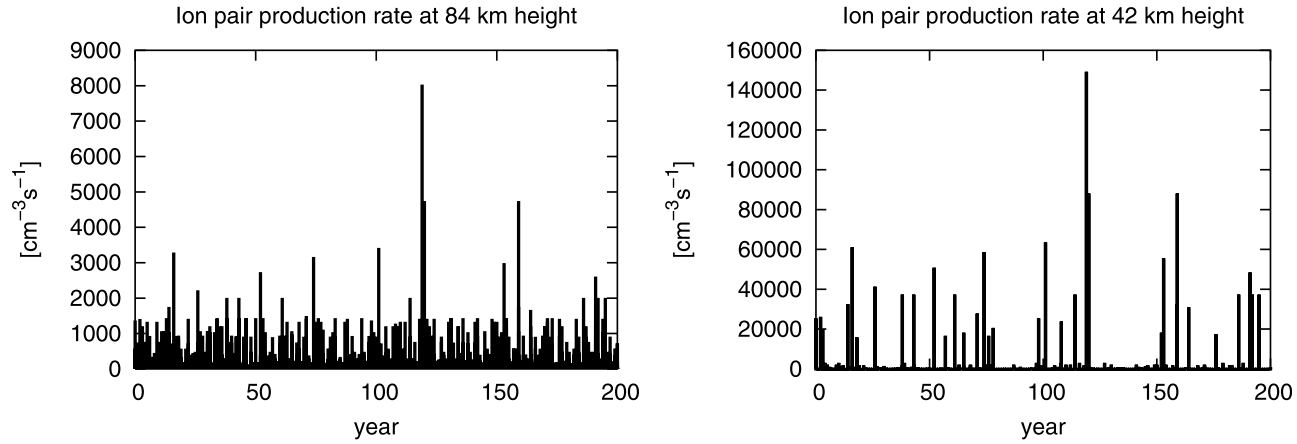

Figure 1. Ion pair production rates (daily averaged values) provided by the simulated 200-year time series of SPEs at 84 and 42 km, respectively.

[*Valet et al.*, 2005], and in simulated reversals the dipole moment drastically decreases [e.g., *Glatzmaier and Roberts*, 1995]. The impact on the geomagnetic shielding efficiency against charged particles from space was investigated by *Vogt et al.* [2007]. Motivated by that study, several characteristic field scenarios have been chosen to be analyzed here with respect to impacts on the atmosphere. The field scenarios are given in section 2.3.

[7] Ozone is a relevant atmospheric absorber of ultraviolet radiation, and hence a reduction of ozone can lead to an increase of harmful shortwave radiation at the Earth's surface especially in the UVB regime. In section 3.1 the modeled impacts on total ozone are shown, and the associated effects on ultraviolet fluxes at the surface are shown in section 3.2.

2. Model Description

2.1. Long Time Series of Solar Particle Events

[8] Direct observations of precipitating solar energetic particles are available only for a few solar cycles but not on timescales of centuries as required for this study which aims to investigate mean values of ozone losses on longer timescales. Such a long-term database can be established with a stochastic simulation as suggested by *Steinhilber* [2005]. The intention of that simulation is to provide long-term databases of solar proton fluxes, including background and smaller solar energetic particle (SEP) events; it is not intended to simulate individual SEP events. Owing to interplanetary scattering and the continuous particle acceleration at traveling interplanetary shocks, SEP events last much longer than the parent solar flare. Thus particles from different solar flares can blend into one long-lasting event, as has been the case for the October 1989 and the October/November 2003 events. Occasionally, such long-lasting periods of high solar fluxes have been termed superevents [e.g., *Müller-Mellin et al.*, 1986; *Dröge et al.*, 1992]. Some events, such as the August 1972 and 14 July 2000 events, lead to rather isolated increases in proton flux and clearly stick out in the particle record, but in active periods such as October 1989 the contribution of individual events to the entire particle profile cannot be identified unambiguously. Thus the simulation is not based on events but on daily averages of particle spectra which are determined with the method described in detail by *Schröter et al.* [2006]. Databases are the IMP and GOES data (from 1973 to 2005). The distribution of spectra and total energy input into the atmosphere, as well as conditional probabilities for a certain total energy dependent on the energy input on the previous day are determined from these data. The histogram is extended to higher energies using the information about solar events from the nitrate layers in ice cores provided by *McCracken et al.* [2001a]. While the satellite data are ordered as daily averages, the accumulation of the nitrate layers basically involves an integration over longer time periods. The event size distributions from satellite observations and from the ice core data have to be related. Only the August 1972 event, an individual event in which the bulk of protons arrived at Earth within 1 d [*Reagan et al.*, 1981], and the October 1989 events, resembling superevents, are contained in both sets of observations. While for the latter event the integrating effect in the nitrate layer certainly plays a role, in the former the integration time is similar to the daily averages obtained from the satellite observations. Therefore the August 1972 event is used to combine the two size distributions for solar events. Owing to this method all extremely large events taken from the ice core data are treated in the simulation in such a manner that the total particle inventory of this event precipitates during 1 d. During the simulation, for each day a value for the total energy and a corresponding spectrum are randomly selected from the combined event size distribution considering the conditional probabilities and considering (1) the energy input during the previous days and (2) the energy input a few thousand days earlier. The first dependence leads to distributions of time period lengths of enhanced fluxes comparable to the ones observed in interplanetary space, while the second dependence leads to a quasi-cyclic behavior of the occurrence of particle events resembling the distribution of times of enhanced particle fluxes over the solar cycle.

[9] From the simulated time series of proton fluxes, atmospheric ionization rates have been calculated by a Monte Carlo simulation of ionizing and dissociative interactions of the protons with air molecules. A detailed description of the method is given by *Schröter et al.* [2006]. The resulting time series of daily ion pair production rates is shown in Figure 1. In comparison with

ionization rates due to SPEs during recent decades [e.g., *Jackman et al.*, 2007] the daily averaged ion pair production rates of the simulated time series occasionally yield dramatically high values. The reasons are threefold.

[10] 1. The time series of nitrate events in ice cores indicates that there had been larger SPEs and times of significantly higher SPE frequencies within the last centuries than during recent solar cycles [*McCracken et al.*, 2001a, 2001b]. For instance, the >30 MeV proton fluence caused by the white light flare of September 1859 was larger by a factor of up to 8 than the fluence of the August 1972 event and was larger by a factor of 6.5 than the fluence due to the October 1989 event [*Thomas et al.*, 2007]. The nitrate proxy data also show that within a period of only 4 years in the 1890s at least three large SEP events occurred, each of which had a fluence exceeding that of the August 1972 flare. The time period singled out in this study might show unusually high ionization rates by the standards of present-day satellite observations; however, it is only a representation of what has been inferred from 400 years worth of nitrate layers in ice cores.

[11] 2. Long-lasting events tend to be concentrated into 1 or 2 d of increased flux which might add another factor of 2 or 3 to the maximum fluxes. Although this changes the instantaneous response of the atmosphere, the effect on timescales of months does not differ depending on whether all particles are injected within 1 d or distributed over a few days.

[12] 3. The ionization rates have been calculated by considering protons with energies up to 500 MeV. For comparison, for example, *Vitt and Jackman* [1996] have used an upper energy limit of 289 MeV. The additional higher-energy particles lead to increased ion pair production rates below about 45 km after major events.

2.2. Atmospheric Model

[13] The atmospheric chemistry model consists of a Single-Layer Isentropic Model of Chemistry and Transport (SLIMCAT) [*Chipperfield*, 1999] derivative as the photochemical module and the two-dimensional meteorological module THIN AIR [*Kinnersley*, 1996]. The latter calculates zonally averaged temperature, pressure, wind fields, and the transport of 37 chemical species on a grid of 29 isentropic and 19 latitudinal levels. The corresponding vertical resolution is about 3 km up to approximately 100 km in height, and the latitudinal resolution is 9.47°. THIN AIR has a gravity wave scheme and parameterizations for the eddy fluxes; a detailed description is given by *Kinnersley* [1996]. The radiative scheme of the model is interactive with the chemistry model in a sense that heating and cooling rates are calculated on the basis of the trace gas amounts of the most important radiative active species (H_2O, N_2O, CH_4, O_3, and NO_2) provided by the model's chemistry scheme. Anthropogenic emissions of CFCs and greenhouse gases are set to represent an industrial atmosphere around the year 2000. The model's transport time step is 3 h, and short-lived species are not treated independently but are treated as "families," e.g., NO_x. The short-lived HO_x is not transported. Every 24 h the chemistry code SLIMCAT is executed. SLIMCAT also uses a family approach for NO_x, HO_x, O_x = ($O(^3P)$,$O(^1D)$,O_3), ClO_x = (Cl, ClO, $2Cl_2O_2$), and BrO_x = (Br, BrO). The partitioning among the family members is calculated by assuming steady state conditions. This approach is quite reasonable in the stratosphere and allows a moderate integration time step of 15 min. However, in the mesosphere the family approach is not valid because reactions interconverting family members are slower. Comparisons with a modified SLIMCAT version without family treatment have shown that the differences in terms of SPE impacts on total ozone are negligible. Therefore it is justified to use the less time-consuming family version which provides a suitable model for the long-term investigations addressed here. A detailed description of SLIMCAT, the included species, the reactions relating them, and the model's treatment of heterogeneous reactions is given by *Chipperfield* [1999]. The model is basically the same as the one used in the previous study of magnetic field variations by *Sinnhuber et al.* [2003]. The reaction rates and absorption cross sections utilized by the model have been updated to the Jet Propulsion Laboratory [*Sander et al.*, 2006] recommendations. The chemical effect of precipitating energetic protons is prescribed by NO_x, HO_x, and O productions depending on the number of ion pairs produced. The ion pair production rates originate from the simulated SPE time series (section 2.1). Basic parameterizations are used to relate these ionization rates to production rates of NO_x, HO_x, and O; this approach is comparable to the one of *Jackman et al.* [2000, 2001, 2005]. Following *Porter et al.* [1976], NO_x formation is set to be 1.25 molecules per ion pair produced, and the branching ratio between $N(^4S)$ and $N(^2D)$ is 45%:55%. $N(^2D)$ rapidly reacts via $N + O_2 \rightarrow NO + O$; in the model it is therefore assumed that $N(^2D)$ instantaneously becomes NO. The branching ratio for $N(^4S)$ and $N(^2D)$ is of importance because there is a direct loss of N and NO through reaction $N(^4S) + NO \rightarrow N_2 + O$. Thus the net NO_x production sensitively depends on the branching ratio [*Brasseur and Solomon*, 2005]. The chosen numbers are in accordance with the values given by *Rusch et al.* [1981], and they are also used, for example, by *Semeniuk et al.* [2005].

[14] Because of the complex water ion cluster chemistry the production factors for HO_x depend on water concentrations as well as on several other parameters such as the abundance of atomic oxygen. The simplified reaction scheme delineated by *Solomon et al.* [1981] is used to calculate these factors online with the chemistry model. The production factors are very similar to the values used by *Jackman et al.* [2005].

[15] Finally, the direct release of atomic oxygen is assumed to be 1.15 atoms per ion pair produced [*Porter et al.*, 1976]. This production of atomic oxygen is of minor importance for SPE impacts, but it was implemented for the sake of completeness.

2.3. Magnetic Field Scenarios

[16] We have set up some magnetic field configurations characteristic for different realistic cases, without claiming that they are real geohistorical ones. As the reference a completely shielded atmosphere without any SPE impact is used, and all differences are with respect to this base configuration. See Table 1 for an overview of the scenarios. Scenario A basically represents the present-day configuration, with $\lambda_c = 60°$, and the geomagnetic axis tilted by 11° with respect to the geographic axis. Here λ_c is assumed to be energy-independent. Because of the tilt the magnetic field's topography translates into zonally averaged shielding

Table 1. Magnetic Field Scenarios[a]

Scenario	Description
base configuration	completely shielded atmosphere, no SPEs
A	present-day dipole configuration, $\lambda_c = 60°$
B	greatly reduced dipole, $\lambda_c = 42°$
C	rotated dipole, $\lambda_c = 60°$, equatorial polar caps
D	pure quadrupole, polar caps $\lambda_c = 60°$ plus equatorial belt of ±10° latitude
E	dipole-quadrupole superposition, north $\lambda_c = 60°$ and south $\lambda_c = 30°$

[a]For details, see text (section 2.3).

factors in the two-dimensional atmospheric model.

[17] B stands for a very weak dipole field with the same tilt, ignoring any quadrupole or higher field parts. Its cutoff latitude corresponds to a dipole moment M of approximately 10% of the topical field strength when the scaling relation for dipolar magnetospheres $\cos\lambda_c \propto M^{-1/6}$ [*Siscoe and Chen*, 1975] is applied. This approximative scaling can be used as long as the field is dominated by its dipole component though this simple approach neglects the fact that the actual sizes of the magnetically open polar caps depend on the field line merging efficiency which is again a function of the north-south component of the interplanetary field; for details, see *Vogt et al.* [2007] and *Zieger et al.* [2006].

[18] Setting C is a dipole configuration of present field strength but is rotated in a way that the polar caps are centered at the equator. This represents a hypothetical reversal situation without any reduction of the magnetic field strength.

[19] Scenarios D and E originate from the investigations of polar cap sizes by *Vogt et al.* [2007]. D stands for an axis-symmetric quadrupole field. A pure axis-symmetric quadrupole field yields open field line regions around the poles and also in the equatorial zone. One particular north-south orientation of the interplanetary magnetic field (IMF) yields a polar cap in one hemisphere and an additional equatorial band of open field lines, and the opposite IMF orientation opens the polar cap in the other hemisphere. However, since the solar wind is highly variable on the long timescales considered here, we combine these two principal configurations to get scenario D: The caps are chosen to have the same cutoff latitude as in case A, and the open field line region in the equatorial zone is assumed to cover a latitudinal range of ±10°. Scenario E is a superposition of a dipole field with a quadrupole field. The quadrupole and the dipole contributions have the same magnetic field strength at the poles, and the dipole strength is approximately 10% of the present-day value. This configuration has two opposing magnetically open cap regions of different sizes in north and south. It is a special case of field superpositions; for details, see *Vogt et al.* [2007] (especially Figures 4 and 5 therein). While in the northern region the field strengths add up, the cap size in the south is much larger. This last field scenario has been adjusted to have the same northern λ_c as scenario A. The cutoff latitude in the south then has a dramatically lower value of 30°.

3. Results and Discussion

[20] Beginning in year 119 of the simulated time series, there is a very active period of large SPEs occurring within a few years (Figure 1). Figure 2 shows the resulting increase of NO_y after the largest events of that active phase in regions which are open to particle precipitation, namely, the southern polar region for the present-day field configuration A and the equatorial region for the axis-symmetric quadrupole D. The differences are with respect to the undisturbed reference atmosphere base configuration, and this applies to all differences shown in this section, unless noted otherwise. While in both cases the ion pair production is similar, the NO_y-enriched air is more efficiently transported downward, and the NO_y decay is slower in the polar region than at the equator. This is especially the case for the

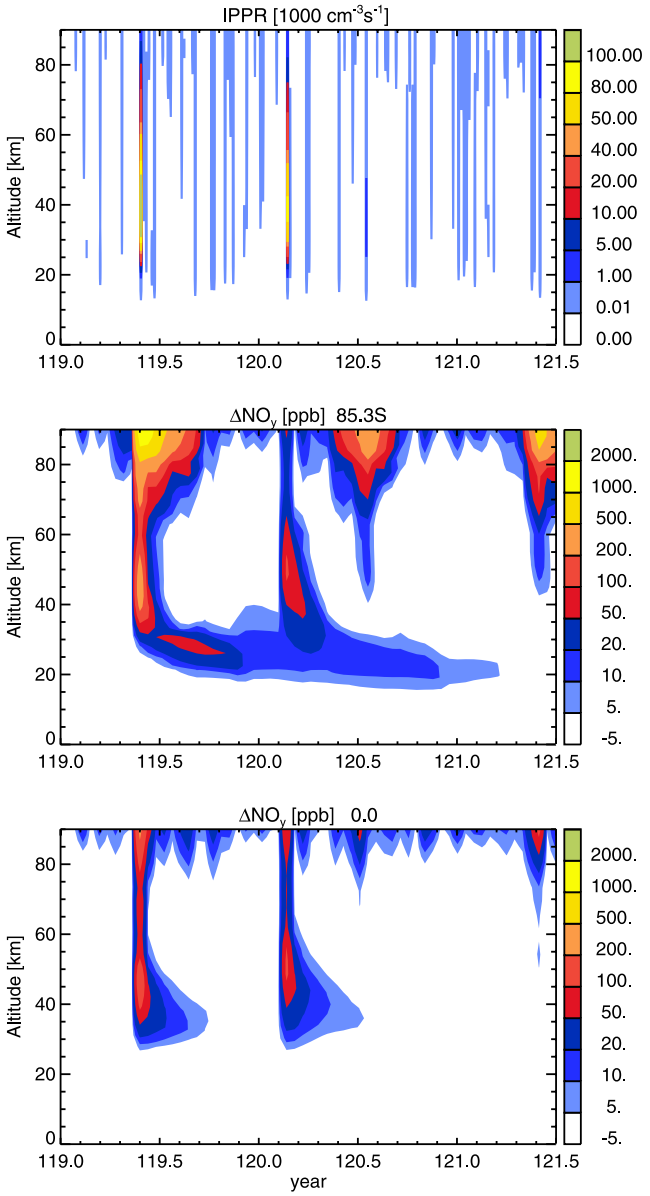

Figure 2. Eighteen months during the very active time period of the simulated time series around model year 120. (top) Ion pair production rates (IPPR) as they are applied to atmospheric regions which are open to particle precipitation (5-d maximum values shown to avoid a too fuzzy picture). Modeled increase of NO_y mixing ratios (middle) in the southern polar region (for scenario A) and (bottom) at the equator (for D).

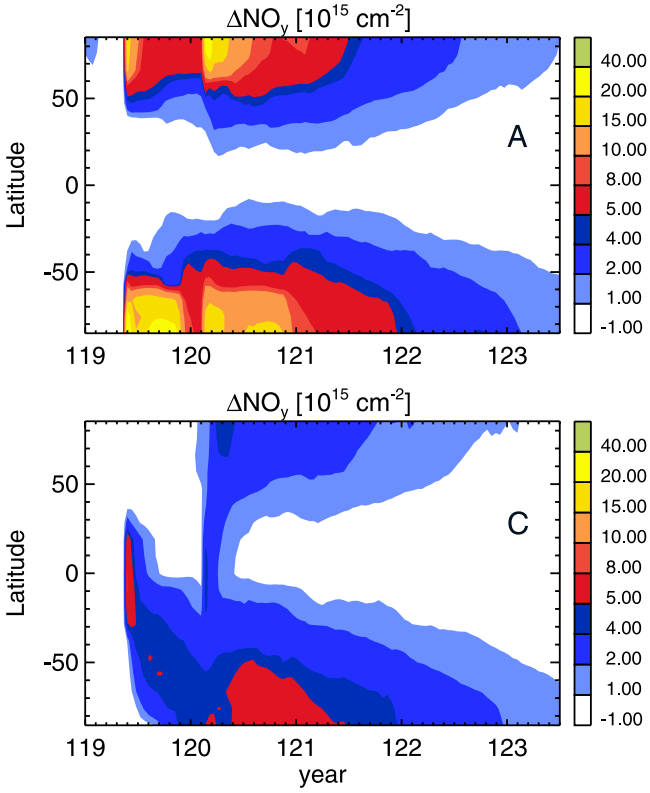

Figure 3. Modeled total atmospheric NO_y column increase as a function of time and latitude during some years of the very active time period of the simulated SPE time series. Results for the (top) present geomagnetic field configuration (scenario A) and (bottom) scenario C which is the equatorial dipole of same cusps size.

large event in model year 119.5 during southern polar night, but enhanced stratospheric NO_y mixing ratios also persist into polar summer.

[21] The model results also indicate that for scenario D, NO_y is significantly increased in the tropical stratosphere for several months after very large events which deposit a considerable amount of energy below the stratopause. This is due to the fact that photochemical lifetimes of the NO_y can reach months below about 40 km [e.g., *Brasseur and Solomon*, 2005]. Figure 3 displays how the increased abundance of NO_y evolves for the case of open field lines in the polar regions and solely in the tropics, respectively. In the latter case, there is propagation of enhanced NO_y on timescales of several months from low latitudes into the polar regions. The differences in NO_y correspond to distinct impacts on ozone. In the case of precipitating particles in the polar regions the effect on ozone is much stronger than it is at lower latitudes. Figure 4 compares the impacts on ozone in the southern polar region and at the equator. In the tropics, ozone losses occur at higher stratospheric altitudes where the bulk of NO_y increase is located, whereas in the lower stratosphere ozone increases. These rising ozone mixing ratios correspond to increased amounts of reservoir species such as $ClONO_2$ and $BrONO_2$. The model atmosphere represents an industrial atmosphere with high stratospheric halogen load which in the case of increasing nitric oxide concentrations after a SPE leads to the formation of reservoir species through $ClO + NO_2 + M \rightarrow ClONO_2 + M$, with an analogous process for $BrONO_2$, by which ozone-depleting halogen substances are transferred into inactive ones. This mechanism has been pointed out by *Jackman et al.* [2000]. On average the simulations only show an increase of lower stratospheric ozone at lower latitudes for scenarios C and D which have open field lines in the tropics, but not for the other scenarios at higher latitudes; see Figure 5.

3.1. Total Ozone

[22] Figure 6 shows the modeled decrease of the total ozone column (TOC) as a function of geographical latitude for the current magnetic field configuration (A) relative to the undisturbed reference atmosphere (base configuration) for 200 years of the simulated SPE time series. The SPE-caused ozone destructions are most pronounced in the polar regions, and although the shielding by the Earth's magnetic field is the same in both hemispheres, the ozone losses in the southern polar region are significantly higher than the ones in the Arctic. These interhemispheric differences are due to unequal atmospheric transport conditions. Strength and the seasonal characteristics of the meridional circulation differ in both hemispheres. Additionally, the polar vortex is stronger in the southern polar region than in the Arctic. This inhibits the ozone influx from lower latitudes more drastically, and, on average, ozone needs a longer time to recover

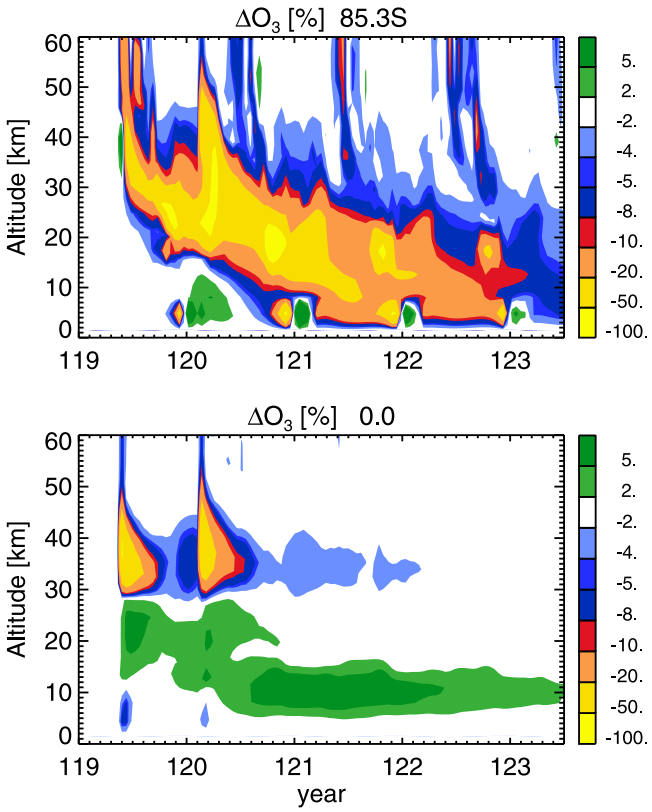

Figure 4. Modeled ozone differences during some years of the very active time period of the simulated SPE time series in the southern polar region for scenario A and at the equator for scenario C.

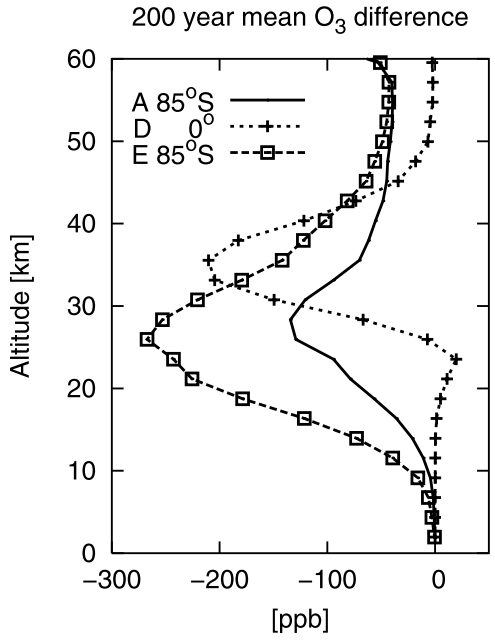

Figure 5. Modeled 200-year averages of ozone differences for some selected scenarios and latitudes.

after a SPE. Figure 6 also shows the TOC reduction during and several years after the intense SPE phase around model year 120 for the shielding scenario A.

[23] The total ozone losses for all other field configurations during the same time period can be seen in Figure 7. In the case of the strongly reduced dipole configuration (B) the larger polar cap areas cause more NO_x and HO_x production in polar and subpolar regions leading to stronger ozone destruction. For scenario C, the rotated dipole of current strength, the results are different in an illustrative way. This case has the same magnetic polar cap size as scenario A, and therefore the production of NO_x and HO_x is similar. However, with C the ozone-depleting radicals are not released in the (geographical) polar regions but in the tropics where they experience stronger photochemical destruction and hardly any descent into the lower stratosphere. The resulting TOC decreases are clearly smaller than for A, and the total ozone losses in the tropics are just marginally higher. The bulk of O_3 loss is again found in the polar regions (Figure 7), strongest in the second half of model year 120 and at the beginning of year 121 in the southern polar region. This corresponds to the NO_y abundance (Figure 3) and indicates the role of the atmospheric poleward transport and subsequent subsidence into the polar ozone layer. This is also confirmed by the model results for scenario D which has the same polar cap size as A and an additional equatorial band open to particle precipitation. Again, the largest TOC reduction is found in both polar regions (Figure 7). The patterns produced by D are quite similar to the patterns of B. Configuration E has a very large magnetic polar cap centered around the South Pole, and consequently, the TOC reduction in the southern polar region is the highest of all scenarios, exceeding 30% for more than 1 year.

[24] A comparison of all scenarios' mean TOC depletion as a function of latitude is shown in Figures 8 and 9 for time periods of 200 years and 5.5 years, respectively. The latter corresponds to an interval of about half a solar cycle beginning in the middle of model year 119 and covers the most intense solar maximum period of the simulated SPE time series. The averaged ozone losses are largest in the southern polar region for all considered field scenarios. In all cases except for C, greater TOC decreases at high latitudes are computed than for the current field configuration. For the magnetic field scenarios B, D, and E the ozone losses caused by large events reach values of ozone hole conditions; for example, the peak ozone loss of E in the southern polar region exceeds 170 Dobson units (DU); its 5.5-year mean value is larger than 60 DU in comparison to about 20 DU for scenario A. In contrast to ozone holes the depletions due to SPEs are not restricted to winter and

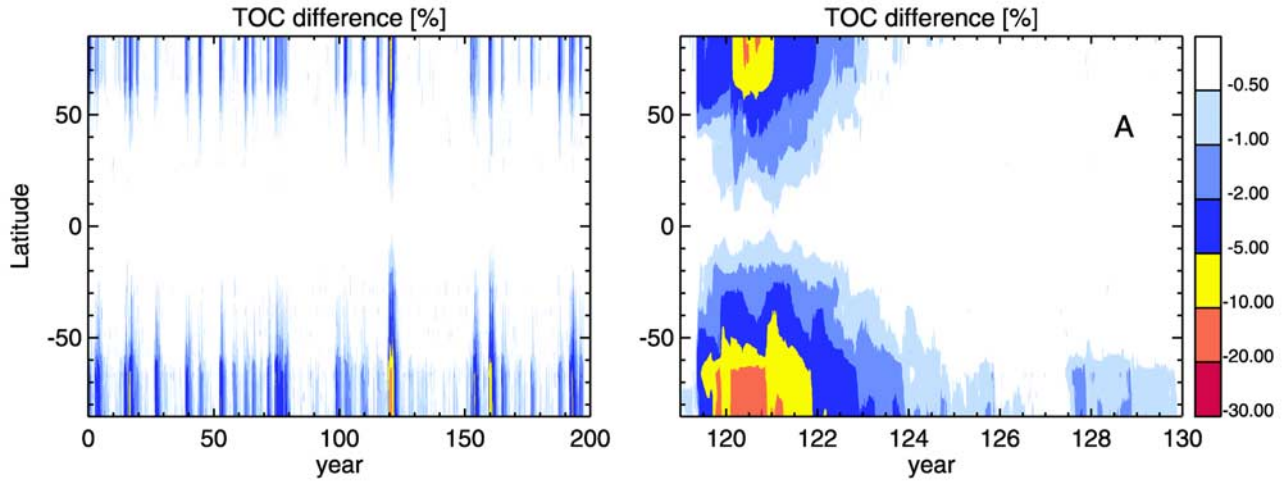

Figure 6. Modeled reduction of the total ozone column (TOC) in percentage for the present-day magnetic field configuration (scenario A with respect to the undisturbed reference atmosphere base configuration; see Table 1 and section 2.3 for a description of the magnetic field scenarios): (left) 200 years of the simulated SPE time series and (right) 11 years during and after the intense SPE period starting at the end of model year 119.

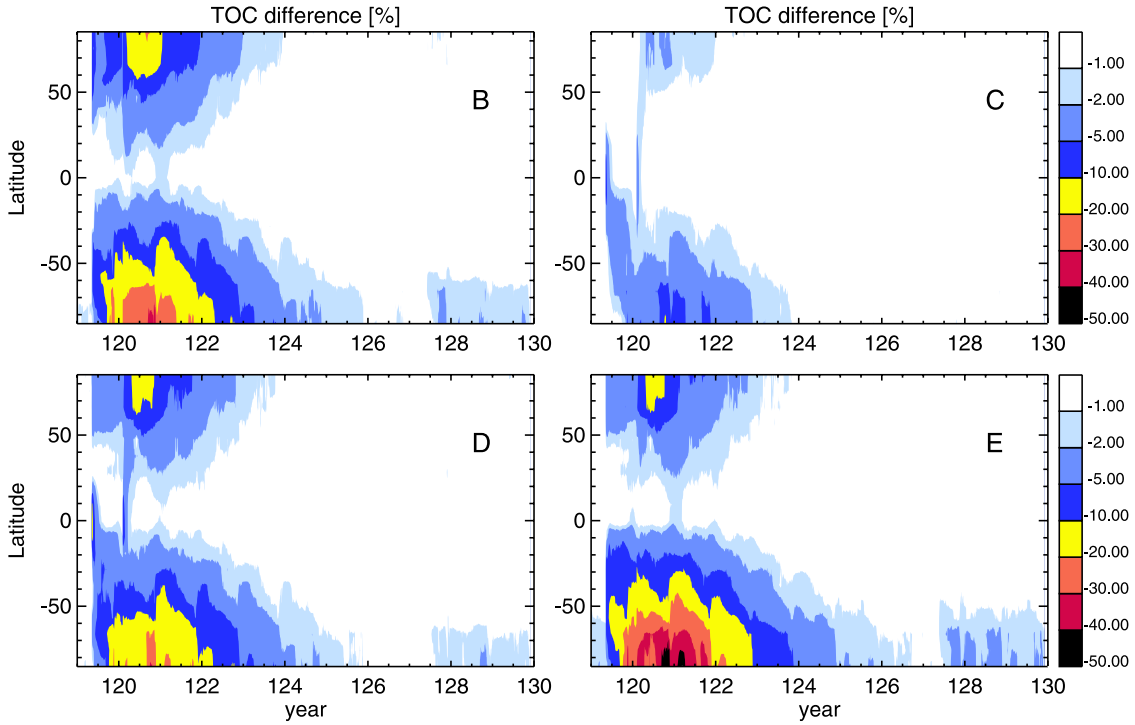

Figure 7. Percentage decrease of the TOC for the scenarios B to E during and several years after the intense SPE period starting at the end of model year 119 corresponding to Figure 6 (right). In year 119 and at the beginning of year 120 the signals of two very large events can be seen in the tropics for cases C and D.

spring times but persist into polar summer because the photochemical lifetime of NO_y is long enough in the middle and lower stratosphere.

3.2. Surface UV

[25] The ozone losses discussed in section 3.1 give rise to an increase of shortwave radiation at the Earth's surface. The actual effect strongly depends on the particular wavelength region. Because of the ozone's strong absorption in the Hartley bands the radiation in the UVB regime (280–315 nm) is very sensitive to ozone changes. Shorter wavelengths are effectively absorbed by molecular oxygen, and therefore the UVC (100–280 nm) fluxes at sea level are quite small and not significantly affected by ozone changes. On the other hand, UVC photons are rather potent in causing harmful effects, and thus this spectral range should not be ignored entirely. In the UVA region (315–400 nm) the biological impacts are smaller but should also be taken into account. For some comments on more technical UV exposure criteria, see *Sliney* [2000]. Though there are some uncertainties concerning the detailed harmfulness of ultraviolet radiation of different wavelengths, it is clear that exposure to UV radiation can cause several acute and chronic health effects on the skin, on the eyes, and on the immune system. Two of the most dramatic effects are increasing risks of skin cancer and cataracts. A suitable measure of the effective shortwave radiation exposure is the UV Index

$$\mathrm{IUV} = \mathrm{k} \int_{\lambda_1}^{\lambda_2} \mathrm{E}(\lambda)\mathrm{S}(\lambda)\, \mathrm{d}\lambda,$$

where λ denotes the wavelength, $E(\lambda)$ is the spectral irradiance, and $S(\lambda)$ is a dimensionless weighting function accounting for the wavelength-dependent potency of the radiation. For different purposes, respective weighting functions and intervals of integration can be used. To assess the UV impact on skin, the erythemal reference action spectrum by the *Commission Internationale de l'Eclairage* [1998] is commonly used for $S(\lambda)$, and the integration interval is 250–400 nm. With $k = 40$ W m^{-2}, IUV becomes the dimensionless solar UV index recommended by the *World Health Organization* [2002] for which the maximum $E(\lambda)$ around noon is used.

[26] In order to estimate the impacts of the ozone losses discussed in section 3.1 on IUV the radiative transfer module SCIARAYS [*Kaiser*, 2001; *Kaiser and Burrows*, 2003] has been utilized. Originally, this program had been developed to support retrievals of atmospheric parameters from limb-scattering measurements by the Scanning Imaging Absorption Spectrometer for Atmospheric Cartography instrument [*Bovensmann et al.*, 1999] on board the European environmental satellite Envisat. For our purpose it is used to yield $E(\lambda)$ at ground level for clear-sky conditions. The atmospheric model results in the form of O_3 profiles, concentrations of several other trace gases, and temperature and pressure values are used as input data for SCIARAYS. The solar spectral irradiance applied on the top of the atmosphere is a measured daily-averaged spectrum (UARS Solar Stellar Irradiance Comparison Experiment [*Rottman et al.*, 1993]) for 2 February 1992.

[27] The solar radiation reaching the Earth's surface greatly depends on the solar zenith angle. In order to

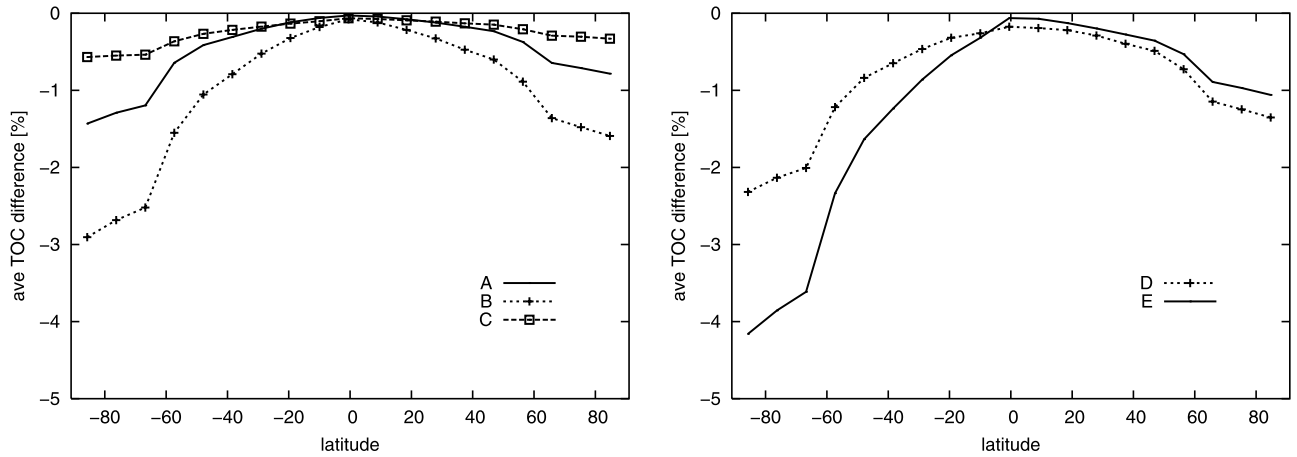

Figure 8. The 200-year averages of SPE causing TOC decrease in percentage versus geographical latitude for the scenarios A–E described in Table 1 and section 2.3.

account for the different conditions in each season the radiative transfer simulations were performed for averaged atmospheric profiles of trace gases of the respective quarter year. In each case the lowest seasonal solar zenith angle at the particular latitude was applied to yield the maximum IUV. Averaging the four seasonal values roughly estimates an annual mean of IUV (the radiative transfer simulations are quite time-consuming, and the strict calculation of averages over several years would cause unreasonable computing expenses).

[28] The calculated relative IUV increases (not shown) correspond fairly with the averaged relative TOC decreases (Figures 8 and 9) for all scenarios. The radiation amplification factor (RAF) which denotes the relative increase of IUV divided by the relative decrease of the TOC lies between 0.95 and 1.3. The lowest values belong to highest solar zenith angles, which is due to the so-called Umkehr effect outlined by the *World Meteorological Organization* [1999]. The values for the RAF given there are in accordance with our findings.

[29] Figure 10 shows the relative IUV changes with respect to the present-day field configuration represented by scenario A. While for the scenarios B, D, and E the IUV increases, especially at middle and high latitudes, for the equatorial dipole C the ultraviolet index decreases almost everywhere. Only in the tropics does the latter scenario yield some slight IUV increase. The tropical IUV increase is largest for the axis-symmetric quadrupole field. The IUV increase at low latitudes, though smaller in terms of relative changes, might be of importance because it adds to already high IUV values.

4. Conclusions

[30] For the first time, different geomagnetic field configurations, which are realistic representations for reversal situations, have been analyzed with respect to their influence on atmospheric impacts of solar proton events. Additionally, enabled by a simulated realistic 200-year time series of SPEs, effects on longer timescales could be investigated for the first time. Our simulations have shown that geomagnetic field variations can have considerable effects on the ozone destruction caused by solar proton events. In all magnetic shielding scenarios the ozone losses on longer timescales are most pronounced in the polar regions which indicates the importance of the photochemical lifetimes of NO_y and its downward transport into the ozone layer. Ozone destruction is for all considered scenar-

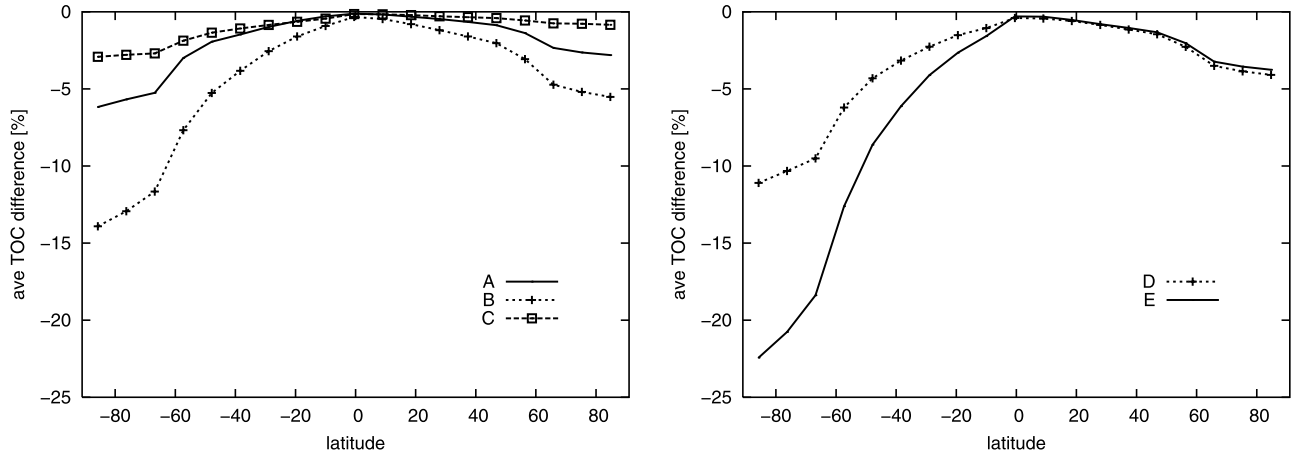

Figure 9. Like Figure 8 but for averages for a time period of 5.5 years during the very active SPE phase starting at the end of year 119 in the simulated time series.

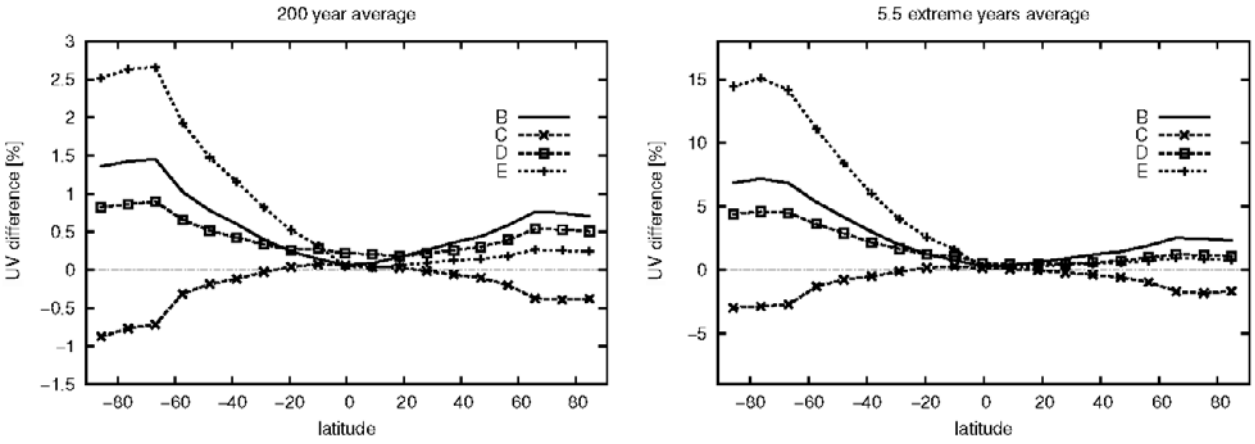

Figure 10. Relative change of ultraviolet indices for the different scenarios with respect to the present-day configuration of scenario A: (left) 200-year averages and (right) mean values for the 5.5 very active years beginning at the end of model year 119.

ios larger in the Southern Hemisphere because of unequal atmospheric transport conditions.

[31] The ozone losses are found to increase with the magnetic polar cap size and with its nearness to the polar regions. In this sense the current field configuration with its small tilt of geomagnetic to geographic axis can be regarded as almost a worst-case situation for the present field strength. The same cap size in the tropics would cause much lower ozone destructions. The scenario of the equatorial dipole of actual cap size can be regarded as a snapshot of a hypothetical geomagnetic reversal with current field strength. As field reversals are very likely connected to field weakenings, they correspond to the other investigated scenarios of weaker fields which lead to significantly enhanced ozone depletions. For these magnetic field configurations, very large events are able to cause dramatic ozone losses especially in the polar regions, lasting for several months up to years. Subsequently, harmful ultraviolet radiation increases at ground level. The absolute ozone losses are smaller at midlatitudes and in the tropics, but because of smaller solar zenith angles the increases of erythemal weighted ultraviolet radiation might also be of importance in these regions.

[32] These results gain importance on the timescales of Earth's magnetic field changes. For instance, in the case of a full field reversal for thousands of years the protecting ozone layer in the polar regions would be reduced to a notable extent, and consequently, UV fluxes would increase significantly for the whole time period of the reversal.

[33] **Acknowledgments.** This work is financially supported by the German Research Council (Deutsche Forschungsgemeinschaft (DFG)) within its priority program "Geomagnetic variations: Spatio-temporal structure, processes, and effects on system Earth" (SPP 1097). H. W. is supported through the grants SI 1088/1-3; J. V., B. Z., A. S., and K. H. G. are supported through VO-855/2 and GL-142/12; and M. B. K. is supported through KA-1297/2. B. Z. also acknowledges support by the Hungarian Scientific Research Fund under contract NI 61013. The SCIARAYS code was kindly provided by J. Kaiser.

References

Birch, M. J., J. K. Hargreaves, A. Senior, and B. J. I. Bromage (2005), Variations in cutoff latitude during selected solar energetic proton events, *J. Geophys. Res.*, *110*, A07221, doi:10.1029/2004JA010833.

Bovensmann, H., J. P. Burrows, M. Buchwitz, J. Frerick, S. Noël, V. V. Rozanov, K. V. Chance, and A. P. H. Goede (1999), SCIAMACHY: Mission objectives and measurement modes, *J. Atmos. Sci.*, *56*, 127–150.

Brasseur, G. P., and S. Solomon (2005), *Aeronomy of the Middle Atmosphere: Chemistry and Physics of the Stratosphere and Mesosphere*, 3rd revis. ed., Springer, New York.

Chipperfield, M. P. (1999), Multiannual simulations with a three-dimensional chemical transport model, *J. Geophys. Res.*, *104*, 1781–1805.

Commission Internationale de l'Eclairage (1998), Erythema reference action spectrum and standard erythema dose, *Rep. ISO 17166:1999/CIE Std S007/E1998*, Vienna.

Crutzen, P. J., I. S. Isaaksen, and G. C. Reid (1975), Solar proton events: Stratospheric sources of nitric oxide, *Science*, *189*, 457–458.

Dröge, W., R. Müller-Mellin, and E. W. Cliver (1992), Superevents: Their origin and propagation through the heliosphere from 0.3 to 0.35 AU, *Astrophys. J.*, *387*, L97–L100.

Fraser-Smith, A. C. (1987), The centered and eccentric geomagnetic dipoles and their poles, 1600–1985, *Rev. Geophys.*, *25*, 1–16.

Glassmeier, K. H., J. Vogt, A. Neuhaus, and S. Buchert (2004), Concerning long-term geomagnetic variations and space climatology, *Ann. Geophys.*, *22*, 3669–3677.

Glatzmaier, G. A., and P. H. Roberts (1995), A three-dimensional self-consistent computer simulation of a geomagnetic field reversal, *Nature*, *377*, 203–209.

Guyodo, Y., and J.-P. Valet (1999), Global changes in intensity of the Earth's magnetic field during the past 800 kyr, *Nature*, *399*, 249–252, doi:10.1038/20420.

Jackman, C. H., A. R. Douglass, R. B. Rood, R. D. Peters, and P. E. Meade (1990), Effect of solar proton events on the middle atmosphere during the past two solar cycles as computed using a two-dimensional model, *J. Geophys. Res.*, *95*, 7417–7428.

Jackman, C. H., E. L. Fleming, and F. M. Vitt (2000), Influence of extremely large solar proton events in a changing stratosphere, *J. Geophys. Res.*, *105*, 11,659–11,670.

Jackman, C. H., R. D. McPeters, G. J. Labow, E. L. Fleming, C. J. Praderas, and J. M. Russel (2001), Northern Hemisphere atmospheric effects due to the July 2000 solar proton event, *Geophys. Res. Lett.*, *28*, 2883–2886.

Jackman, C. H., M. T. DeLand, G. J. Labov, E. L. Fleming, D. K. Weisenstein, M. K. W. Ko, M. Sinnhuber, and J. M. Russell (2005), Neutral atmospheric influences of the solar proton events in October–November 2003, *J. Geophys. Res.*, *110*, A09S27, doi:10.1029/2004JA010888.

Jackman, C. H., D. R. Marsh, F. M. Vitt, R. R. Garcia, E. L. Fleming, G. J. Labow, C. E. Randall, M. López-Puertas, and B. Funke (2007), Short- and medium-term atmospheric effects of very large solar proton events, *Atmos. Chem. Phys. Discuss.*, *7*, 10,543–10,588.

Kaiser, J. W. (2001), *Atmospheric Parameter Retrieval From UV-vis-NIR Limb Scattering Measurements*, Logos, Berlin.

Kaiser, J. W., and J. P. Burrows (2003), Fast weighting functions for retrievals from limb scattering measurements, *J. Quant. Spectrosc. Radiat. Transfer*, *77*, 273–283.

Kinnersley, J. S. (1996), The climatology of the stratospheric 'Thin Air' model, *Q. J. R. Meteorol. Soc.*, *122*, 219–252.

Lary, D. J. (1997), Catalytic destruction of stratospheric ozone, *J. Geophys. Res.*, *102*, 21,515–21,526.

Mankinen, E. A., and G. B. Dalrymple (1979), Revised geomagnetic polarity time scale for the interval 0–5 m.y B.P., *J. Geophys. Res.*, *84*, 615–626.

McCracken, K. G., G. A. M. Dreschhoff, E. J. Zeller, D. F. Smart, and M. A. Shea (2001a), Solar cosmic ray events for the period 1561–1994: 1. Identification in polar ice, 1561–1950, *J. Geophys. Res.*, *106*, 21,585–21,598.

McCracken, K. G., G. A. M. Dreschhoff, D. F. Smart, and M. A. Shea (2001b), Solar cosmic ray events for the period 1561–1994: 2. The Gleissberg periodicity, *J. Geophys. Res.*, *106*, 21,599–21,609.

McElhinny, M. W., and W. E. Senanayake (1982), Variations in the geomagnetic dipole 1: The past 50,000 years, *J. Geomagn. Geoelectr.*, *34*, 39–51.

Merrill, R. T., and P. L. McFadden (1999), Geomagnetic polarity transitions, *Rev. Geophys.*, *37*, 201–226.

Müller-Mellin, R., K. Röhrs, and G. Wibberenz (1986), Super-events in the inner solar system and their relation to the solar cycle, in *The Sun and the Heliosphere in Three Dimensions: Proceedings of the Nineteenth ESLAB Symposium*, pp. 349–354, D. Reidel, Dordrecht, Netherlands.

Nicolet, M. (1970), Ozone and hydrogen reactions, *Ann. Geophys.*, *26*, 531–546.

Porter, H. S., C. H. Jackman, and A. E. S. Green (1976), Efficiencies for production of atomic nitrogen and oxygen by relativistic proton impact in air, *J. Chem. Phys.*, *65*, 154–167.

Randall, C. E., D. E. Siskind, and R. M. Bevilaqua (2001), Stratospheric NO_x enhancements in the Southern Hemisphere vortex in winter/spring of 2000, *Geophys. Res. Lett.*, *28*, 2385–2388.

Reagan, J. B., R. E. Meyerott, R. W. Nightingale, R. C. Gunton, R. G. Johnson, J. E. Evans, W. L. Imhof, D. F. Heath, and A. J. Krueger (1981), Effects of the August 1972 solar particle events on stratospheric ozone, *J. Geophys. Res.*, *86*, 1473–1494.

Rohen, G., et al. (2005), Ozone depletion during the solar proton events of October/November 2003 as seen by SCIAMACHY, *J. Geophys. Res.*, *110*, A09539, doi:10.1029/2004JA010984.

Rottman, G. J., T. N. Woods, and T. P. Sparn (1993), Solar-Stellar Irradiance Comparison Experiment 1: 1. Instrument design and operation, *J. Geophys. Res.*, *98*, 10,667–10,677.

Rusch, D. W., J.-C. Gérard, S. Solomon, P. J. Crutzen, and G. C. Reid (1981), The effect of particle precipitation events on the neutral and ion chemistry of the middle atmosphere–I: Odd nitrogen, *Planet. Space Sci.*, *29*, 767–774.

Sander, S. P., et al. (2006), Chemical kinetics and photochemical data for use in atmospheric studies: Evaluation number 15, *JPL Publ.*, *06-2*.

Schröter, J., B. Heber, F. Steinhilber, and M.-B. Kallenrode (2006), Energetic particles in the atmosphere: A Monte-Carlo simulation, *Adv. Space Res.*, *37*, 1597–1601.

Semeniuk, K., J. C. McConnell, and C. H. Jackman (2005), Simulation of October–November 2003 solar proton events in the CMA GCM: Comparison with observations, *Geophys. Res. Lett.*, *32*, L15S02, doi:10.1029/2005GL022392.

Seppälä, A., P. T. Verronen, V. F. Sofieva, J. Tamminen, E. Kyrölä, C. J. Rodger, and M. A. Cliverd (2006), Destruction of the tertiary ozone maximum during a solar proton event, *Geophys. Res. Lett.*, *33*, L07804, doi:10.1029/2005GL025571.

Sinnhuber, M., J. P. Burrows, M. P. Chipperfield, C. H. Jackman, M.-B. Kallenrode, K. F. Künzi, and M. Quack (2003), A model study of the impact of magnetic field structure on atmospheric composition during solar proton events, *Geophys. Res. Lett.*, *30*(15), 1818, doi:10.1029/2003GL017265.

Siscoe, G. L., and C.-K. Chen (1975), The paleomagnetosphere, *J. Geophys. Res.*, *80*, 4675–4680.

Sliney, D. H. (2000), Ultraviolet radiation exposure criteria, *Radiat. Prot. Dosim.*, *91*(1–3), 213–222.

Solomon, S., D. W. Rusch, J.-C. Gérard, G. C. Reid, and P. J. Crutzen (1981), The effect of particle precipitation events on the neutral and ion chemistry of the middle atmosphere: II. Odd hydrogen, *Planet. Space Sci.*, *29*, 885–892.

Solomon, S., G. C. Reid, D. W. Rusch, and R. J. Thomas (1983), Mesospheric ozone depletion during the solar proton event of July 13, 1982, part II. Comparison between theory and measurements, *Geophys. Res. Lett.*, *10*, 257–260.

Steinhilber, F. (2005), Simulation der solaren Aktivität auf Zeitskalen von Solarzyklen bis zu Jahrhunderten, diploma thesis, Univ. of Osnabrück, Osnabrück, Germany.

Swider, W., and T. J. Keneshea (1973), Decrease of ozone and atomic oxygen in the lower mesosphere during a PCT event, *Planet. Space Sci.*, *21*, 1969–1973.

Thomas, B. C., C. H. Jackman, and A. L. Melott (2007), Modeling atmospheric effects of the September 1859 solar flare, *Geophys. Res. Lett.*, *34*, L06810, doi:10.1029/2006GL029174.

Valet, J.-P., L. Meynadier, and Y. Guyodo (2005), Geomagnetic dipole strength and reversal rate over the past two million years, *Nature*, *435*, 802–805, doi:10.1038/nature03674.

Verronen, P. T., A. Seppälä, M. A. Cliverd, C. J. Rodger, E. Kyrölä, C.-F. Enell, T. Ulich, and E. Turunen (2005), Diurnal variation of ozone depletion during the October–November 2003 solar proton events, *J. Geophys. Res.*, *110*, A09S32, doi:10.1029/2004JA010932.

Verronen, P. T., A. Seppälä, E. Kyrölä, J. Tamminen, H. M. Pickett, and E. Turunen (2006), Production of odd hydrogen in the mesosphere during the January 2005 solar proton event, *Geophys. Res. Lett.*, *33*, L24811, doi:10.1029/2006GL028115.

Vitt, F. M., and C. H. Jackman (1996), A comparison of sources of odd nitrogen production from 1974 through 1993 in the Earth's middle atmosphere as calculated using a two-dimensional model, *J. Geophys. Res.*, *101*, 6729–6739.

Vogt, J., B. Zieger, K.-H. Glassmeier, A. Stadelmann, M.-B. Kallenrode, M. Sinnhuber, and H. Winkler (2007), Energetic particles in the paleomagnetosphere: Reduced dipole configurations and quadrupolar contributions, *J. Geophys. Res.*, *112*, A06216, doi:10.1029/2006JA012224.

von Clarmann, T., N. Glatthor, M. Höpfner, S. Kellmann, R. Ruhnke, G. P. Stiller, H. Fischer, B. Funke, S. Gil-López, and M. López-Puertas (2005), Experimental evidence of perturbed odd hydrogen and chlorine chemistry after the October 2003 solar proton events, *J. Geophys. Res.*, *110*, A09S45, doi:10.1029/2005JA011053.

Wicht, J., and P. Olson (2004), A detailed study of the polarity reversal mechanism in a numerical dynamo model, *Geochem. Geophys. Geosyst.*, *5*, Q03H10, doi:10.1029/2003GC000602.

World Health Organization (2002), Global solar UV index: A practical guide, *Rep. WHO/SDE/OEH/02.2*, Geneva, Switzerland.

World Meteorological Organization (1999), Scientific assessment of ozone depletion: 1998, report, Geneva, Switzerland.

Zieger, B., J. Vogt, and K.-H. Glassmeier (2006), Scaling relations in the paleomagnetosphere derived from MHD simulations, *J. Geophys. Res.*, *111*, A06203, doi:10.1029/2005JA011531.

K.-H. Glassmeier and A. Stadelmann, Institut für Geophysik und Meteorologie, Technische Universität Braunschweig, Mendelssohnstr 3, D-38106 Braunschweig, Germany. (kh.glassmeier@tu-bs.de; a.neuhaus@tu-bs.de)

M.-B. Kallenrode, Department of Physics, Universität Osnabrück, Barbarastraße 7, D-49076 Osnabrück, Germany. (mkallenr@uni-osnabrueck.de)

J. Notholt, M. Sinnhuber, and H. Winkler, Institute of Environmental Physics, University of Bremen, Otto-Hahn-Allee 1, D-28334 Bremen, Germany. (jnotholt@iup.physik.uni-bremen.de; miriam@iup.physik.uni-bremen.de; hwinkler@iup.physik.uni-bremen.de)

F. Steinhilber, Swiss Federal Institute of Aquatic Science and Technology (Eawag), SE-8600 Dubendorf, Switzerland. (friedhelm.steinhilber@eawag.ch)

J. Vogt, School of Engineering and Science, Jacobs University Bremen, Campus Ring 8, P.O. Box 750561, D-28759 Bremen, Germany. (j.vogt@iu-bremen.de)

B. Zieger, Department of Atmospheric, Oceanic and Space Sciences, University of Michigan, Ann Arbor, MI 48109, USA. (zieger@ggki.hu)